Quantum Hall effect transition in scanning gate experiments

A. Baumgartner,[*] T. Ihn, and K. Ensslin[†]

Solid State Physics Laboratory, ETH Zurich, 8093 Zurich, Switzerland

K. Maranowski and A. C. Gossard

Materials Department, University of California, Santa Barbara, California 93106, USA

We present systematic scanning gate studies on a two-dimensional electron gas in the regime of the quantum Hall effect (QHE). We observe the macroscopic Hall bar response as a function of the local variation of the potential landscape in order to investigate the QHE transition. At even integer filling factors, no changes can be introduced by the local perturbation, consistent with the robustness of the QHE. Between two QHE plateaus such local changes induce sharp features in the Hall resistance images. We observe two distinct $1/B$-periodic patterns, one in the low-field part and one in the high-field part of the transition. The crossover between the patterns is smooth, with both coexisting at a characteristic filling factor. We distinguish experimentally different Hall bar responses to the perturbations, for example, in the nonlocal Hall resistance. Based on our experimental findings we draw an intuitive picture of the QHE transition as a percolation transition of edge states and their coupling at saddle points of the local potential.

I. INTRODUCTION

One of the most intriguing phenomena in solid state physics is the quantum Hall effect (QHE)[1,2] found in two-dimensional electron gases (2DEGs). The quantization of the Hall plateaus is independent of the characteristics of individual samples, which is the reason why this effect is used as the international resistance standard.[3] The transition between QHE states is also a well accessible model system for two-dimensional quantum phase transitions and important for theoretical considerations.[4]

A wealth of experiments on the QHE can be found in the literature, many of them interpreted in terms of edge channels,[5,6] for example, backscattering at (macroscopic) potential barriers and constrictions.[7–10] In similar experiments also some insight into the self-consistent stripe structure of the QHE states[11] can be gained.[12,13] However, for the formation of quantum Hall plateaus and the transition between them, local potential fluctuations in the sample interior play a major role. Macroscopic transport experiments provide only information about averaged properties and have to be interpreted statistically.[14] Experiments with selectively populated edge channels have shown the importance of individual impurities for edge state equilibration and backscattering[15,16] and in mesoscopic structures this should be true in an even greater context. There is a reason to believe that individual scattering centers also play an important role in the breakdown of the QHE.[17] In order to identify individual scattering sites and corresponding microscopic mechanisms experimentally, scanning probe techniques offer new experimental opportunities.

Only very few scanning probe experiments at the required low temperatures and high magnetic fields have been performed up to now. Scanning a single-electron transistor across the surface allowed the imaging of the electrochemical potential and the striped structure of the quantum Hall state and to map localized states in both the integer and fractional QHE regimes.[18–21] Local electron transport across incompressible strips at fluctuations of the local potential have been studied with the "scanning charge accumulation" technique.[22,23] These techniques give insight into the microscopic details of the QHE states.

In this paper we present experiments in which we influence the QHE state locally and investigate the response on the Hall voltage in an actual device. The employed "scanning gate" technique consists of applying a dc voltage to the metallic tip of an atomic force microscope (AFM) which is brought in close proximity to the electronic structure to be investigated. The tip acts like a local gate which is scanned above the sample surface while the resistance is recorded for every position. Direct evidence of scattering at individual potential fluctuations was observed in previous experiments monitoring the equilibration length and the longitudinal resistance as function of the tip position.[24] In other experiments two edge states could be coupled directly by the scanned tip.[25] In direct measurements on a Hall bar the coupling of edge states could be quantified in the framework of the Landauer-Büttiker formalism.[26]

Here, the sensitivity of the Hall resistance to local potential perturbations is investigated systematically. The coupling of edge states occurs as a concerted effect of individual potential fluctuations present naturally, and the potential induced by the AFM tip. Such experiments are of fundamental interest since they provide a connection between the edge channel picture and the view of a percolating network of localized states in the bulk.

The article is structured as follows: the setup, sample, and the experimental technique are discussed in Sec. II. In Sec. III various scanning gate experiments in the QHE regime of a conventional Hall bar are presented, described, and compared in some detail. Section IV discusses these results in a qualitative model based on the idea of a percolation transition for the QHE transition.
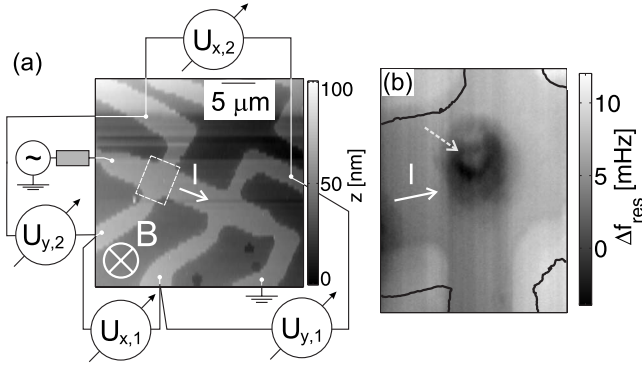
FIG. 1. (a) Topographic image of a typical sample recorded at a temperature of 1.9 K. The schematic shows the setup for the resistance measurements and the white rectangle the area of the actual experiments. (b) Shift in the resonance frequency of the tuning fork sensor for a scan at a constant height of 120 nm. In both figures the white arrow indicates the current direction.

II. MEASUREMENT SETUP AND SAMPLES

Most of the presented experiments were done on a Hall bar ("sample A") of $W=4$ μm width and $L=10$ μm length between the voltage contacts. The Hall bar was etched in a GaAs/AlGaAs heterostructure with a 2DEG 52 nm below the surface. The electron density was $n=3.6\times10^{15}$ m^{-2}, the mobility $\mu=66$ m^2/Vs, and the mean-free path $\ell=6.5$ μm at liquid He temperatures. A low-temperature topography scan is shown in Fig. 1(a). For the tip-voltage dependent experiments "sample B" was used, a Hall bar of nominally identical design with $n=5.0\times10^{15}$ m^{-2} and $\mu=9$ m^2/Vs. An ac current at the frequency $f_m=680.9$ Hz and amplitude $I=100$ nA was applied, as indicated by the white arrows in Fig. 1. The voltages $U_{x,1}$ and $U_{x,2}$ along the Hall bar, and the Hall voltage $U_{y,2}$ were measured by lock-in amplifiers. The Hall voltage on the right Hall cross, $U_{y,1}$, can be inferred using Kirchhoff's voltage law. All experiments were done at a temperature of 1.9 K. Magnetic fields of up to 8 T can be applied perpendicular to the sample surface.

An electrochemically sharpened PtIr tip kept at constant voltage with respect to the electron gas is scanned across the sample surface at a constant height of $d=120$ nm with a homebuilt low-temperature scanning probe microscope and a quartz tuning fork force sensor.[27,28] The longitudinal and Hall voltages are recorded during each scan for a grid of tip positions, leading to the "scanning gate images." If not mentioned otherwise, the tip voltage was $U_{tip}=0.0$ V for all measurements, which corresponds to a voltage of ~-0.3 V with respect to the 2DEG because of the contact potential difference between the two materials. It proved essential not to apply strong negative and positive voltages in order to avoid persistent inhomogeneities in the sample. We ensured that the sample properties have not changed during the experiments by repeatedly taking standard magnetoresistance curves after a few scans.

Typical scans take about 2 h due to the low bandwidth of the resistance measurements. During the experiments, shifts in the resonance frequency of the tuning fork sensor are recorded, which allows us to exclude that features in the scan-

ning gate images originate from changes in the tip-sample geometry or from surface charging. On the example shown in Fig. 1(b), like on all images presented in this paper, the topographic contour of the Hall bar is superposed as black lines. It is extracted from a topographic scan taken prior to the experiments. The current direction is indicated as a white arrow. In the frequency shift image one recognizes the Hall cross due to the lower tip-sample distance and an area of reduced signal in the center of the Hall cross (dashed gray arrow). The latter does not correspond to a topographic feature and we attribute it to charged surface states from a series of previous experiments performed at this tip position. These features did not change during the presented experiments. As can be seen in Fig. 1(b), the topographic contour does not exactly coincide with the sample edges determined from the frequency shift because of the tip and sample geometries. The contour lines only serve as a reference for relative positions in all images.

III. EXPERIMENTS

A. Spin degenerate Landau levels

The central result of this paper is the series of scanning gate images presented in Fig. 2, taken on sample A. It was recorded for different magnetic fields, B, corresponding to filling factors between $\nu=8.0$ and $\nu=4.0$, indicated by symbols in Fig. 3. All images presented in this paper have individually adjusted color scales. Figure 3 shows $R_{xx,2}$ and $R_{xy,2}$ as function of B with the tip withdrawn more than 1.3 μm from the sample surface. The magnetic fields for the scans were chosen equidistantly on the longitudinal resistance scale. Figure 3(a) shows Shubnikov–de Haas (SdH) oscillations with well pronounced minima at even integer filling factors, where the resistance drops below the resolution of our measurement. In Fig. 3(b) the Hall resistance is plotted for the same field interval. We observe a notable difference between the fields where the maxima of the Shubnikov–de Haas oscillations occur (vertical lines) and the fields where the Hall resistance increases to half the value between two QHE plateaus.

Area-averaged resistance values obtained from the scans in Fig. 2 are plotted as symbols (blue online) with the corresponding mean deviations from the average as error bars. The values obtained from the scanning gate experiments reproduce the magnetoresistance curves quite well and the tip-induced deviations are small compared to the absolute resistance values. Especially the last finding suggests that the tip is not a very invasive probe and that the scanning gate technique can be used to investigate the quantum Hall states.

The full information is contained in the images in Fig. 2 representing $R_{xy,2}$ as function of the tip position for filling factors $4\leq\nu\leq8$. We observed the same qualitative behavior for the transitions from $\nu=8$ to $\nu=10$ and from $\nu=10$ to $\nu=12$. Lower filling factors will be discussed below. The data in Fig. 2 are arranged following the R_{xx} curves in Fig. 3 and the corresponding filling factor is given below each image. The patterns of tip-induced changes in the Hall resistance
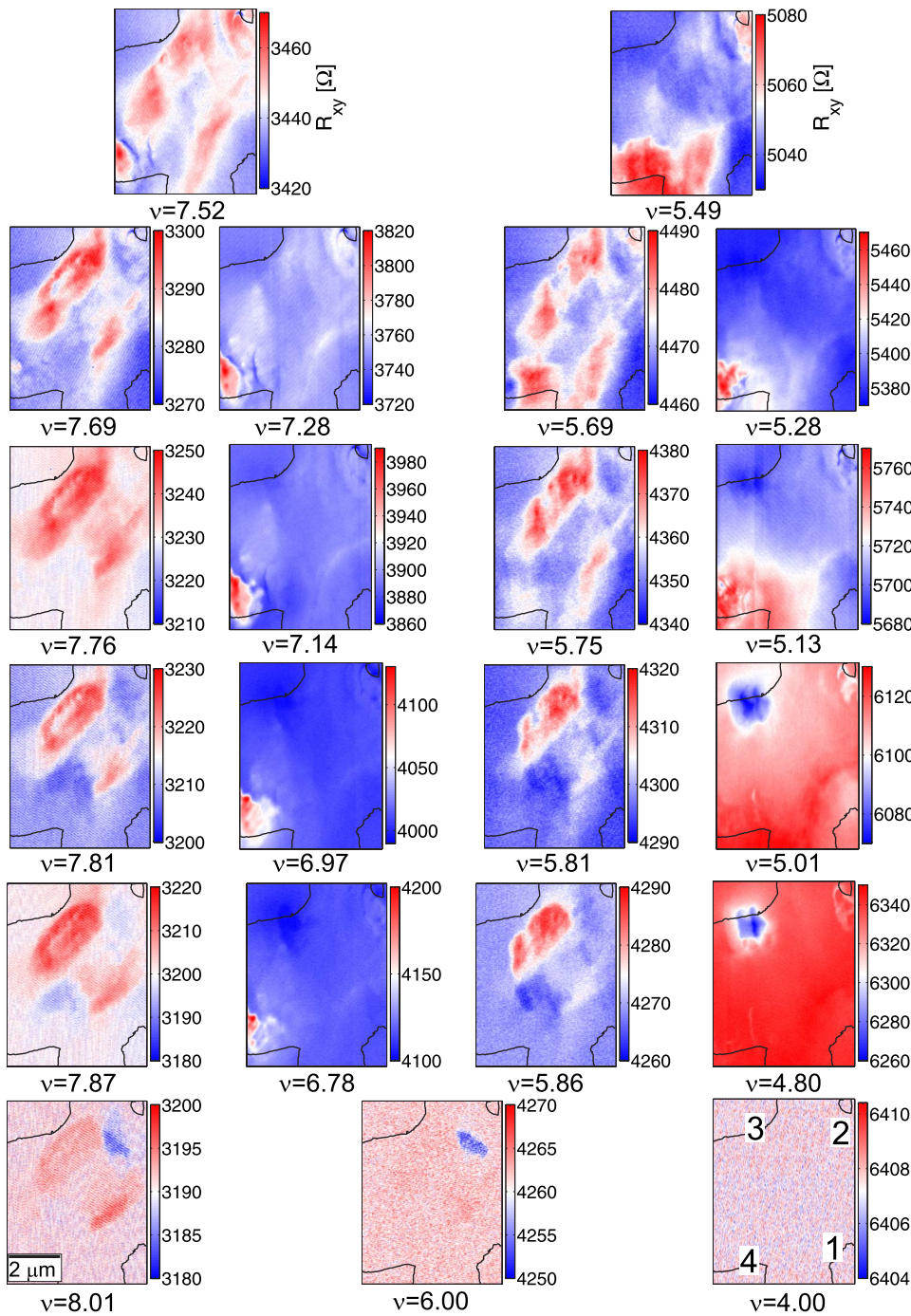
FIG. 2. (Color online) Scanning gate images of $R_{xy,2}$ for two QHE transitions, assembled as on the magnetoresistance curve. The numbers at $\nu=4$ label the corners as used in the text.

strongly depend on the filling factor. The images can be divided into four categories: images recorded (1) at even integer filling factors, (2) at the low-field side of the QHE transition, i.e., filling factors larger than a critical value ν^*, (3) at the high-field side of the transition, $\nu < \nu^*$, and (4) at $\nu \approx \nu^*$, corresponding roughly to the field of maximum longitudinal resistance.

(1) At the even integer filling factor $\nu=4.0$, at the bottom right of Fig. 2, the Hall resistance is not influenced by the AFM tip within the experimental sensitivity. This finding coincides with the notion of the quantum Hall plateaus being independent of the detailed local potential in the sample interior. This image also contains the numbering of the Hall cross corners used to describe the positions of the induced resistance changes in other images later on. The small deviation of the experimental from the theoretical plateau values is due to a constant offset voltage in the setup and the error is smaller than 1.5%. The small local tip-induced Hall resistance changes that can be discerned near corners 1–3 for filling factors $\nu=6.0$ and 8.0 are very faint. They possibly originate from less pronounced SdH minima and a locally slightly decreased filling factor due to the effective tip potential.

(2) At the low-field side of a quantum Hall transition, e.g., between $\nu=8$ and $\nu<7.7$ in Fig. 2, several well-defined local changes in the Hall resistance are observed. Near corners 1
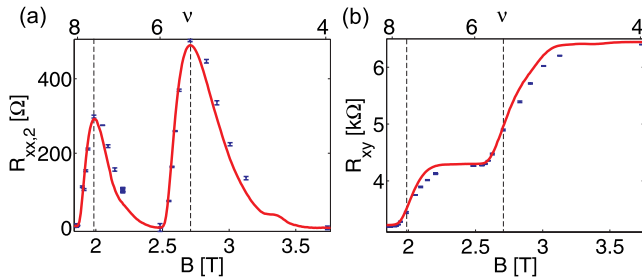
FIG. 3. (Color online) (a) $R_{xx,2}$ and (b) $R_{xy,2}$ plotted versus the magnetic field, B. The individual points represent the mean values of the respective scanning gate experiments presented in Fig. 2. The error bars stand for the standard deviations in each image.

and 3, R_{xy} is enhanced and near the others slightly reduced compared to the unperturbed Hall bar, e.g., when the tip resides well outside the structure. Especially the features with an enhanced resistance exhibit substructure. The tip-induced patterns at magnetic fields corresponding to the next spin degenerate Landau level, between $\nu=6$ and $\nu=5.7$ in Fig. 2, are very similar. This finding demonstrates the $1/B$ periodicity of the transport properties in the quantum Hall regime also in the presence of local potential perturbations. Although the longitudinal resistance varies from essentially zero to almost the maximum of the SdH oscillation in this field interval, the Hall resistance changes only by about 10% of the difference between the two QHE plateaus.

(3) At the high-field side of the quantum Hall transition, i.e., between $\nu=7.3$ and $\nu<6.8$ and between $\nu=5.3$ and $\nu<4.8$ in Fig. 2, a single tip-induced change of the Hall resistance in corner 4 dominates the scanning gate images whereas the pattern observed previously at the low-field side has disappeared. The maximum resistance change in these scans is about three times larger and with sharper spatial variation than individual peaks at the start of the transition. Also this pattern was observed in other transitions with a $1/B$ periodicity. In addition, a new feature arises at filling factor $\nu=5$ near corner 3, which dominates the images at higher fields. This will be discussed in the next section. In this field interval R_{xx} drops from the SdH maximum to zero, while the Hall voltage increases to the next plateau by more than 50% of the total step.

(4) At the characteristic filling factors $\nu^*=7.5$ and $\nu^*=5.7$ in Fig. 2, near the fields where the SdH maxima occur, the two patterns coexist. Around these filling factors a gradual change from one pattern to the other can be observed. A similar description applies to the scanning gate image at $\nu^*=3.8$ shown in Fig. 4.

B. Spin split Landau levels

Magnetoresistance curves between filling factors $\nu=4$ and $\nu=2$ are shown in Fig. 5. They both exhibit a minimum at $\nu=3$, which is expected for the longitudinal resistance. The minimum in the Hall resistance, however, is unusual and its origin is not clear. The absence of quantization is due to the weakness of the spin splitting. The spin splitting also has a strong effect on scanning gate images at these fields, as demonstrated in Fig. 4.
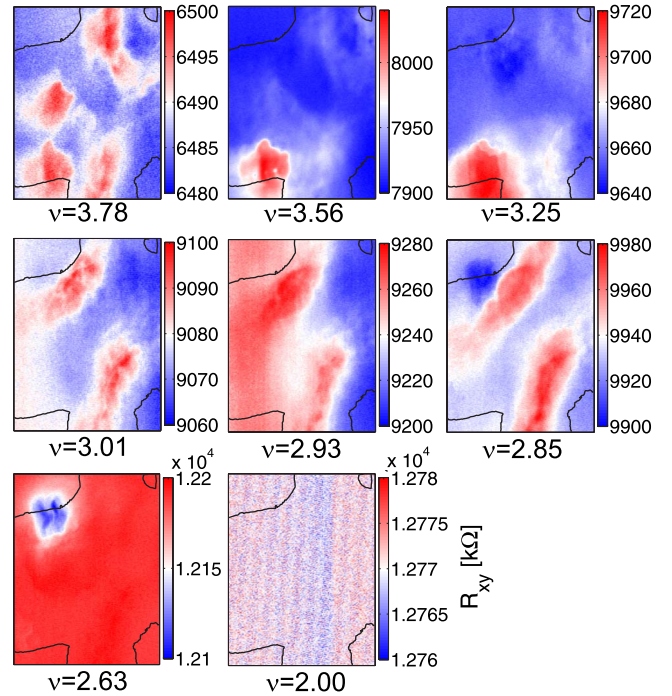

FIG. 4. (Color online) Scanning gate experiments of $R_{xy,2}$ for $4>\nu>2$. The magnetic fields of these measurements are given in Fig. 5.

At $\nu=3.78$ the two patterns of the spin degenerate Landau states coexist, as discussed in the previous section. Here, this regime is shifted to lower fields compared to the SdH maximum. At $\nu=3.56$ the feature of the spin degenerate case of the high-field side of the QHE transition prevails and gets broadened at $\nu=3.25$. At filling factor $\nu=3.0$ a new pattern occurs with features that seem to bend around corners 1 and 3, in contrast to the pattern in the spin degenerate case. At the field where the longitudinal resistance exhibits the next maximum, at $\nu=2.85$, a new feature coexists with the previous, namely, a well localized minimum at corner 3. At $\nu=2.63$ this feature is the only perceptible in the scanning gate image, which is essentially the same as at filling factor $\nu=5.0$ found in Fig. 2. At $\nu=2.0$ no features can be observed as discussed in detail in the previous section.
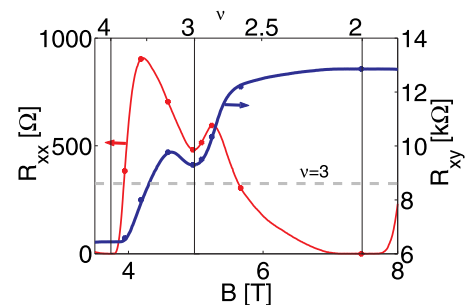

FIG. 5. (Color online) $R_{xx,2}$ and $R_{xy,2}$ for $4>\nu>2$. The magnetic fields at which the experiments of Fig. 4 were taken are indicated as circles.
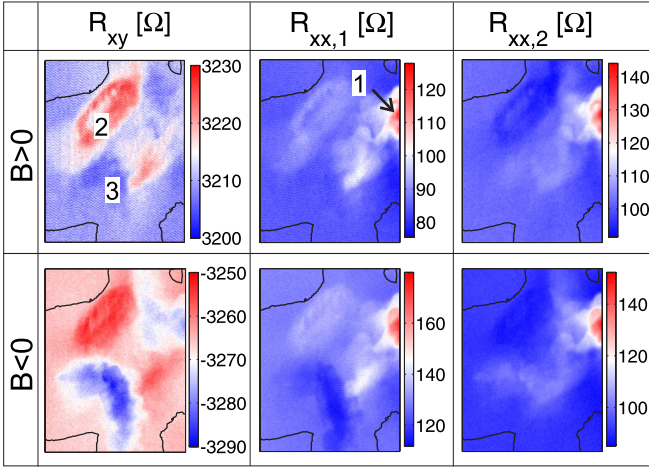
FIG. 6. (Color online) Scanning gate images of $R_{xy,2}$ (left column), $R_{xx,1}$ (central column), and $R_{xx,2}$ (right column) at filling factor $\nu=7.81$ at positive (top row) and at the same but reversed magnetic field (bottom row).

C. Longitudinal resistances and inversion of the magnetic field

The longitudinal resistance is widely used for the characterization of a 2DEG. Here we focus on the tip-induced changes in the corresponding scanning gate images at the position where we observed changes in the Hall resistance. Changes in the local potential of one Hall cross do not necessarily induce changes in the second Hall cross. Kirchhoff's law then requires that the two longitudinal resistances are altered accordingly, not necessarily symmetrically.

In Fig. 6 the scanning gate images for $R_{xy,2} \equiv R_{xy}$, $R_{xx,1}$, and $R_{xx,2}$ (columns) are shown for positive (first row) and negative magnetic fields (second row) at $\nu=7.81$, at the low-field side of a QHE transition.

The change in the resistance labeled with 1 in Fig. 6 occurs in both longitudinal resistances and at both field polarities with equal strength. The filling factors refer to positive

fields. Neither of the Hall resistances shows an appreciable change in this position. The signals for feature 2 (3) are changed to more positive (negative) values for both field polarities in R_{xy} and $R_{xx,1}$, whereas they are reduced for $R_{xx,2}$. Clearly, the responses of the Hall bar to potential changes in those three tip positions are significantly different.

Figure 7 shows scanning gate images for the same quantities as in Fig. 6, but for filling factor $\nu=6.97$ at the high-field side of the QHE transition. At positive field values feature 1 dominates all scanning gate images, while it is very weak at the inverted field. Exactly the opposite is found for feature 2. This contrasts the behavior of all three features in Fig. 6. The different origin of the two features in Fig. 7 becomes also apparent in $R_{xx,1}$ and $R_{xx,2}$ where the two resistance changes have the opposite sign in all four images.

D. Nonlocal resistance changes

A remarkable difference in the response to an external local potential perturbation can be seen in "nonlocal" experiments. Here we use the term nonlocal in the unorthodox sense that the voltage measurement takes place far away from the potential perturbation. In experiments in the classical transport regime resistance changes can be introduced only by perturbing the local potential between the voltage contacts.[32] Any effect of a local perturbation should be reduced *monotonically* and on the length scale of a mean-free path away from the contacts. This picture depends crucially on the assumption that the system can be described by a homogeneous local conductivity tensor.

We construct the nonlocal Hall resistance $R_{xy,1}$ as function of the tip position on the other Hall cross using Kirchhoff's laws, the two longitudinal voltages, $U_{x,1}$ and $U_{x,2}$, and the Hall voltage $U_{y,2}$. A selection of such images is shown in Fig. 8 for some field values also given in Fig. 2.

At all even integer filling factors (not shown) the nonlocal Hall resistance is independent of the tip scanned across the remote Hall cross. Also on the low-field side of the QHE transitions, i.e., for $\nu=7.81$ and $\nu=5.81$ in Fig. 8, hardly any
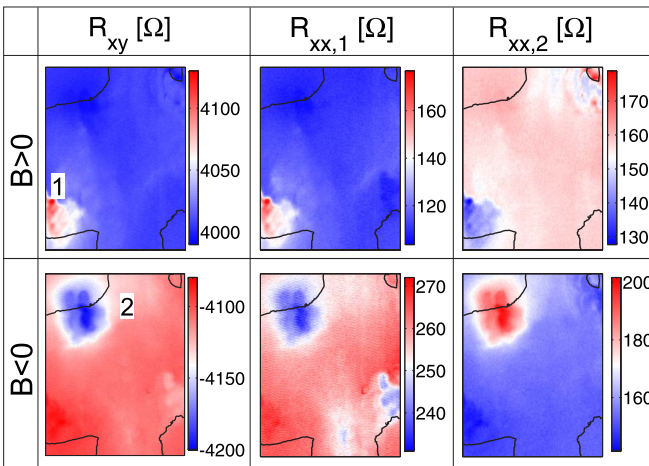

FIG. 7. (Color online) Scanning gate images of $R_{xy,2}$ (left column), $R_{xx,1}$ (central column), and $R_{xx,2}$ (right column) at filling factor $\nu=6.97$ at positive (top row) and at the same but reversed magnetic field (bottom row).
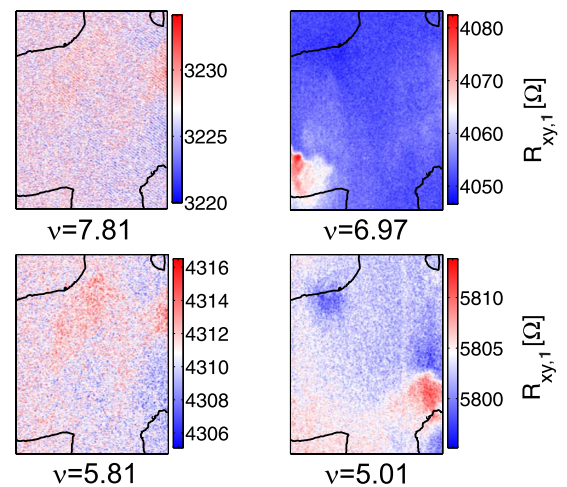

FIG. 8. (Color online) Scanning gate images of the nonlocal Hall resistance $R_{xy,1}$ for the same filling factors as in the lower central row of Fig. 2.

deviation from the unperturbed values can be discriminated. In contrast, on the high-field side, e.g., for ν=6.97 and ν =5.01 in Fig. 8, well resolved features appear at positions where also changes in $R_{xy,2}$ are evident. The latter is also true for the maximum in corner 1, but the corresponding maximum in $R_{xy,2}$ is overshadowed by other resistance changes. No nonlocal resistance changes have been observed in sample B with a lower mobility.

E. Tip-voltage dependence

The dependence of a single scanning gate feature on the applied tip voltage was investigated on sample B, because scans with large potential differences introduce local changes in the sample, presumably by locally charging the surface or the donor layer. Such local charging might explain the increased electron density, reduced mobility, and unsymmetric magnetoresistance curves found in this sample in control experiments. In Fig. 9(a) a series of scans is presented at B =4.25 T, corresponding to $\nu \approx 4.9$. The edges of the Hall cross are again given as dark contours and the current is applied from the top left to the bottom right contact.

In all images the dominant feature is a single maximum at the lower left corner, indicated by a black arrow. For U_{tip} =−0.7 V it has a rather irregular shape, the average radius is larger than a micrometer, and the maximum tip-induced resistance change is more than 500 Ω. With increasing tip voltage the local resistance change becomes more disk shaped and the diameter decreases. The induced resistance change drops to zero between U_{tip}=0.7 V and U_{tip}=0.8 V. Also the width of the feature decreases to values below our resolution. Above U_{tip}=0.8 V no well-defined change of the Hall voltage related to this feature could be observed. We note, however, that there are faint minima and maxima occurring
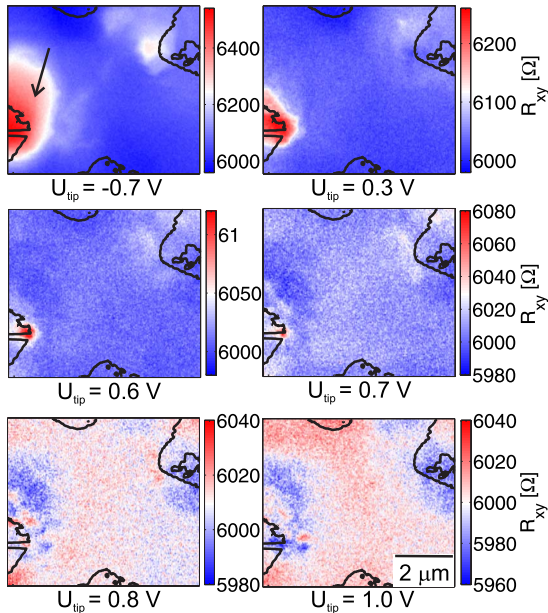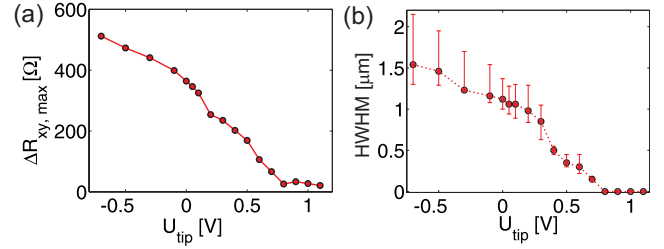

FIG. 10. (Color online) (a) Maximum and (b) half width at half maximum of the main feature observed in Fig. 9 (black arrow) as function of the applied tip voltage U_{tip}. The error bars in (b) indicate the minimum and maximum observed distance of the half-height contour of the feature.

within the region of the feature and a slight decrease compared to the background at this and the opposite corner of the Hall cross present at all voltages.

The maximum induced change in the Hall resistance attributed to this feature and its half width at half the maximum (HWHM) are plotted as function of the applied tip voltage in Fig. 10. The HWHM was extracted by measuring the typical distance of the contour line at half of the maximum from the center of the feature (found at higher voltages), together with the minimum and maximum distances. The latter are plotted as error bars in Fig. 10(b). Both the induced change in resistance and the width of the feature drop monotonically with increasing voltage and drop below the resolution of our setup at $U_{\text{tip}} \approx 0.7$ V. The feature does not recover at more positive voltages. We also note a slight change in the slope of the characteristic radius and a small dip in the induced resistance change at $U_{\text{tip}} \approx 0.2$ V. The deviation from a circular shape increases with increasing feature width at lower voltages. In spite of a flattening of both curves at the lowest applied tip voltages no saturation could be observed.

IV. DISCUSSION

A. QHE transition

The quantum mechanical states of electrons in a 2DEG with a sufficiently smooth potential in high magnetic fields can be approximated as edge states, equipotential lines where the local potential pierces the Fermi energy.[30] Screening leads to a spatial segregation into compressible and incompressible regions.[11] Most often the QHE transition is explained as a localization-delocalization transition in a percolating network of "internal" edge states localized at potential fluctuations. The 2DEG can be modeled as a lattice of saddle points in the potential landscape where in- and outgoing ideally conducting states are coupled.[14,30,31] The Landauer-Büttiker formalism allows one to connect the microscopic picture with measurements on the macroscopic contacts. Büttiker's description depends only on the existence of quantum channels and is independent of where they run exactly. It reproduces directly the quantization of the QHE plateaus and R_{xx}=0 at integer filling factors.[5] The transmission problem of a four-terminal Hall cross can be formulated easily and a basis set for transmission matrices can be constructed for

FIG. 9. (Color online) Scanning gate experiments on sample B at $\nu \approx 4.9$ for a series of tip voltages U_{tip}. The arrow points out the discussed resistance change.
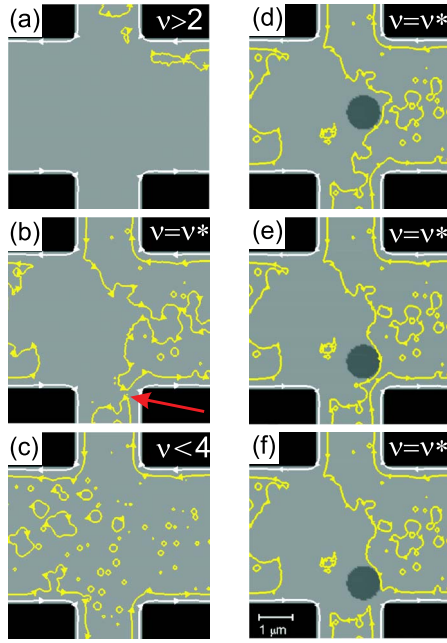
FIG. 11. (Color online) (a)–(c) Schematics of the QHE transition from $\nu \approx 2$ to $\nu \approx 4$. The red arrow in (b) indicates the critical saddle point in the transition. (d)–(f) Effect of a scanned potential perturbation at $\nu = \nu^*$.

characterization, as demonstrated in the Appendix.

Here we briefly discuss in a simple model the QHE transition and its effect on the Hall voltage in a (four-terminal) Hall cross: in Figs. 11(a)–11(c) the QHE transition from $\nu = 2$ to $\nu = 4$ is illustrated for an artificial potential landscape produced by a Hall cross and several hundred $1/r$-shaped potential fluctuations at random positions. The white and yellow equipotential lines represent the ideally conducting Landau states. At a critical filling factor ν^* the percolation of the $\nu = 4$-state through the Hall cross takes place—not necessarily for all contact pairs at the same filling factor, since we deal with a finite system. Figure 11(b) shows the situation where the percolating states are coupled at only a single saddle point in the potential (red arrow). Only at this position a perturbation of the potential leads to a change in the Hall voltage. This is demonstrated in Figs. 11(d)–11(f), where the AFM tip is simulated as a disk of locally enhanced potential which redirects the edge states. Note that there are other saddle points in the system where the Hall voltage is not influenced by the AFM tip.

B. Interpretation of the experiments

The resistance changes in the QHE regime are more strongly localized than in the classical transport regime.[32] The symmetries discussed in Ref. 32 also hold in the QHE regime with the same restraints. These symmetries are not found in the scans discussed here, which we attribute to potential fluctuations that break the symmetry of the Hall cross on the relevant length scale. We therefore conclude that this length scale decreases when entering the QHE regime and the sample should be described by a nonhomogeneous model.

In a very recent publication scanning gate experiments in the regime of the QHE transition have been investigated theoretically, based on a percolation model for a lattice of saddle points with tunneling or ideally conducting links.[29] "Hot spots," i.e., regions of increased sensitivity of the (2-terminal) conductance to local changes in the potential, have been linked to how well the saddle point in question is coupled to *both* contacts. The measurement in a multiterminal arrangement discriminates couplings between more contacts, as shown in the Appendix.

We find experimentally that at even integer filling factors the Hall bar response cannot be altered by a local perturbation. At these fields the model in Ref. 29 suggests that all links in the lattice have zero transmission. A local perturbation merely produces closed loops of conducting links (localized states), disconnected from the contacts, which does not change the measured voltages.

Our picture of the scanning gate experiments is that the tip potential slightly varies the transmission in each saddle point of the potential and the induced resistance changes measure how important this saddle point is for the coupling of the corresponding macroscopic contacts (hot spots). The $1/B$ periodicity seen in Fig. 2 reflects the periodic local density of states at the Fermi energy expected for the local filling of the Landau levels. Also the induced resistance changes are very similar at corresponding filling factors, which supports our interpretation. In Fig. 2 we find two patterns that coexist at roughly the field where the SdH oscillation is maximum. We identify this field with the value of the QHE percolation transition, because of the maximum backscattering in the Hall bar. At the high-field side of the transition essentially only one hot spot, possibly consisting of many not separately resolved saddle points, is observed. These saddle points in this particular sample are active and therefore responsible for roughly 3/4 of the changes in the Hall voltage of each transition. The saddle points producing the second pattern, with more features and different couplings of the contacts, are responsible for the rest of the QHE transition. Above and below the percolation field the position and form of the localized states are completely different, because the former "hot links" become ideally conducting. The different responses to the local perturbation discussed for Figs. 6 and 7 correspond to different transmission matrices in the Landauer-Büttiker picture and describe different couplings between the macroscopic contacts, like it is explained in the Appendix. A simulation of the 2-terminal conductance cannot account for these findings. We do not find that the number of hot spots increases gradually with the approach to the transition, as predicted in Ref. 29, rather we do find the coexistence of the patterns, where all critical saddle points of the transition are active.

From Fig. 10(a) we conclude that the tip potential for electrons increases with more negative voltages applied, which increases the influence on individual saddle points, as it is expected theoretically.[29] Less obvious is the fact that the half width at half maximum also increases, which is not expected for an ideal metal surface. We attribute this effect to the reduced screening capability of the 2DEG, especially in the QHE regime. Qualitatively, more features can be observed in Fig. 2 on the side with lower resistance changes,

consistent with the notion of smaller induced local changes when more saddle points are involved in the coupling of the contacts. For exactly one saddle point governing the transition between the high quantum Hall plateau at $\nu_h = 4$ and the low plateau at $\nu_l = 6$ the largest possible induced change in the Hall resistance is

$$\Delta R_{xy,\text{max}} = \frac{h}{e^2}\left(\frac{1}{\nu_h} - \frac{1}{\nu_l}\right) = 2.15 \text{ k}\Omega. \qquad (1)$$

We did not observe this value which indicates that other hot spots are involved outside the scanned area. Also Eq. (1) only holds if the transmission of the saddle point can be tuned between 0 or 1 without changing the basic shape of the potential. This requirement might not be met when very large negative voltages are applied to the tip. The simulations in Ref. 29 show that the additional coupling at other saddle points reduces the maximum effect and that the average change in conductance saturates at much larger tip voltages than on the most sensitive individual saddle point. Ideally, the resistance changes should vanish for a fully compensated contact potential difference (CPD) between tip and sample. In other experiments we found CPDs between 0.3 and 0.7 eV for this material system,[32,33] in good agreement with the presented data.

Edge states introduce very long equilibration and phase coherence lengths, which can lead to nonlocal resistance changes.[9] The simplest way to explain changes in the nonlocal Hall resistance is to assume a nonideal contact on the second Hall cross.[6] A necessary condition then is that the electrochemical potential of the scattered edge channels is not equilibrated before they enter the next contact. Intuitively, assuming the existence of compressible and incompressible strips[11] with the former carrying the electrochemical potential, this equilibration is weaker for states more separated by incompressible strips, which is the case for filling factors at the high-field end of a QHE transition. This is in accordance with Fig. 8 of our experiments.

In our picture the spin-split states should be understood as independent, but spatially and electrostatically different channels. The coupling of these states occurs at a different fraction of the filling factor (odd integers) and introduces a qualitatively different feature in the scanning gate images, compared to the even integer states. From this we conclude that the actual microscopic structure of the QHE state not only dictates quantitatively the coupling at a given saddle point, but that this structure is also important for the global form of the total network of QHE states and for the QHE transition, e.g., for slight deviations in the critical exponent of the QHE transition.

V. SUMMARY AND CONCLUSION

We investigated the influence of position and amplitude of local potential perturbations on the QHE transition by scanning gate experiments on a small Hall bar. We find pronounced features in the images and an abrupt change in the pattern of the images near half-integer filling factors. All findings, including nonlocal Hall resistance patterns and a characterization method for the individual features, are de-

scribed in the light of an intuitive model of edge states coupled at local saddle points in the 2DEG potential. We expect that scanning gate experiments as presented here can be used to extract real space informations about the potential landscape of 2DEGs by investigating also larger Hall bars, or about phase-coherence phenomena such as (universal) conductance fluctuations in small conductors, e.g., quantum wires. A still strongly debated topic is the breakdown of the quantum Hall effect for large current densities, for which we expect further experimental insight from scanning gate experiments.

APPENDIX

In this appendix we work out an intuitive basis set of transmission matrices for a single Hall cross and calculate the corresponding resistance changes in the Landauer-Büttiker formalism.

Backscattering inside the Hall bar has already been discussed for scanning gate experiments in the literature.[26] The Hall resistances are not altered in this particular case, i.e., $\Delta R_{xy,1} = \Delta R_{xy,2} = 0$, and the changes in both longitudinal resistances are $\Delta R_{xx,1} = \Delta R_{xx,2} = (h/e^2\nu)[\delta/(\nu-\delta)] \equiv R_{xy}^{(0)}[\delta/(\nu - \delta)]$, with δ describing the reduction of transmission in one channel.

The transmission matrix of a single Hall cross has 16 elements and 7 linearly independent relations from current and energy conservation. Therefore we need nine linearly independent matrices to form a basis and nine parameters to form a general transmission matrix. The choice of basis matrices is arbitrary and can, for example, be constructed by considering intuitive examples.

The coupling schemes can be grouped, for example, by the number of edge states that are backscattered into the contact of their origin. The cases where the state in contact 1, 2, or 6 are backscattered do not change any resistances. Backscattering in lead "HB" is equivalent to backscattering in the interior of the Hall bar. In Fig. 12(a) the case is shown where backscattering occurs in two contacts: 6 and the Hall bar HB. Rotations by 90° lead to another three basis matrices. Basically, these cases are already discussed by Büttiker
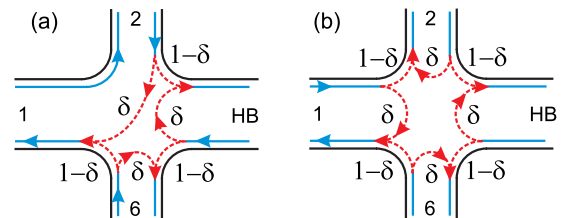

FIG. 12. (Color online) Edge state coupling in a Hall cross with backscattering in (a) contacts 6 and HB and (b) in all four contacts.

as "anomalous quantum Hall effect due to adjacent contacts with internal reflection."[6] There is no possibility for backscattering in exactly three leads and Fig. 12(b) shows the case of backscattering in all four contacts. The corresponding resistance can be found in Table I. The first column indicates the contacts in which the edge states are scattered back. The other columns show the changes in the two longitudinal resistances and the change in the Hall resistance of the corresponding Hall cross, both at positive and reversed magnetic fields. All cases depend only on one parameter δ and the introduced resistance changes have all the same amplitude, $w := R_{xy}^{(0)}[\delta/(\nu-\delta)]$. It is only the last five scattering matrices that produce a change in the local Hall resistance. None leads to changes in the right Hall voltage, i.e., $\Delta R_{xy,1} \equiv 0$. Each of these mechanisms can be distinguished in principle by only three measurements, for example, changes occurring only in the longitudinal resistances correspond to backscattering inside the Hall bar, as found, for example, in the text. It must be highlighted, however, that the choice of the basis matrices is arbitrary and that any linear combination is also a valid transmission matrix and can lead to different characteristics.

TABLE I. Resistance changes for the nine scattering configurations described in the text and depicted in Fig. 12. HB is the Hall bar contact and $w := R_{xy}^{(0)}[\delta/(\nu-\delta)]$.

Scat. leads	$B>0$			$B<0$		
	$\Delta R_{xx,1}$	$\Delta R_{xx,2}$	$\Delta R_{xy,2}$	$\Delta R_{xx,1}$	$\Delta R_{xx,2}$	$\Delta R_{xy,2}$
1	0	0	0	0	0	0
2	0	0	0	0	0	0
6	0	0	0	0	0	0
HB	w	w	0	w	w	0
HB, 6	w	0	w	w	w	0
6, 1	0	0	0	0	w	$-w$
1, 2	w	0	w	0	0	0
2, HB	w	w	0	0	w	$-w$
All	w	0	w	0	w	$-w$

*Present address: School of Physics and Astronomy, University of Nottingham, University Park, Nottingham NG7 2RD, United Kingdom. baumgartner@phys.ethz.ch

†URL: http://www.nanophys.ethz.ch

[1] K. v. Klitzing, G. Dorda, and M. Pepper, Phys. Rev. Lett. **45**, 494 (1980).

[2] D. C. Tsui, H. L. Stormer, and A. C. Gossard, Phys. Rev. Lett. **48**, 1559 (1982).

[3] B. Jeckelmann and B. Jeanneret, Rep. Prog. Phys. **64**, 1603 (2001).

[4] Y. Dubi, Y. Meir, and Y. Avishai, Phys. Rev. Lett. **94**, 156406 (2005).

[5] M. Büttiker, Phys. Rev. B **38**, 9375 (1988).

[6] M. Büttiker, *Semiconductors and Semimetals* (Academic, New York, 1992), Vol. 35, p. 191.

[7] S. Washburn, A. B. Fowler, H. Schmid, and D. Kern, Phys. Rev. Lett. **61**, 2801 (1988).

[8] B. Snell, P. Beton, P. Main, A. Neves, J. Owers-Bradley, L. Eaves, M. Henini, H. Hughes, S. Beaumont, and C. Wilkinson, J. Phys.: Condens. Matter **1**, 7499 (1989).

[9] P. L. McEuen, A. Szafer, C. A. Richter, B. W. Alphenaar, J. K. Jain, A. D. Stone, R. G. Wheeler, and R. N. Sacks, Phys. Rev. Lett. **64**, 2062 (1990).

[10] R. J. Haug, Semicond. Sci. Technol. **8**, 131 (1993).

[11] D. B. Chklovskii, B. I. Shklovskii, and L. I. Glazman, Phys. Rev. B **46**, 4026 (1992).

[12] S. W. Hwang, D. C. Tsui, and M. Shayegan, Phys. Rev. B **48**, 8161 (1993).

[13] Y. Y. Wei, J. Weis, K. v. Klitzing, and K. Eberl, Phys. Rev. Lett. **81**, 1674 (1998).

[14] J. Chalker and P. Coddington, J. Phys. C **21**, 2665 (1988).

[15] B. Alphenaar, P. McEuen, R. Wheeler, and R. Sacks, Physica B **175**, 235 (1991).

[16] Y. Acremann, T. Heinzel, K. Ensslin, E. Gini, H. Melchior, and M. Holland, Phys. Rev. B **59**, 2116 (1999).

[17] L. Eaves, Physica B **298**, 1 (2001).

[18] A. Yacoby, H. Hess, T. Fulton, L. Pfeiffer, and K. West, Solid State Commun. **111**, 1 (1999).

[19] N. B. Zhitenev, T. A. Fulton, A. Yacoby, H. F. Hess, L. N. Pfeiffer, and K. W. West, Nature (London) **404**, 473 (2000).

[20] S. Ilani, J. Martin, E. Teitelbaum, J. H. Smet, D. Mahalu, V. Umansky, and A. Yacoby, Nature (London) **427**, 328 (2004).

[21] J. Martin, S. Ilani, B. Verdene, J. Smet, V. Umansky, D. Mahalu, D. Schuh, G. Abstreiter, and A. Yacoby, Science **305**, 980 (2004).

[22] G. A. Steele, R. C. Ashoori, L. N. Pfeiffer, and K. W. West, Phys. Rev. Lett. **95**, 136804 (2005).

[23] S. H. Tessmer, P. I. Glicofridis, R. C. Ashoori, L. S. Levitov, and M. R. Melloch, Nature (London) **392**, 51 (1998).

[24] M. T. Woodside, C. Vale, P. L. McEuen, C. Kadow, K. D. Maranowski, and A. C. Gossard, Phys. Rev. B **64**, 041310(R) (2001).

[25] T. Ihn, J. Rychen, T. Vančura, K. Ensslin, W. Wegscheider, and M. Bichler, Physica E (Amsterdam) **13**, 671 (2002).

[26] A. Kičin, A. Pioda, T. Ihn, K. Ensslin, D. C. Driscoll, and A. C. Gossard, Phys. Rev. B **70**, 205302 (2004).

[27] J. Rychen, T. Ihn, P. Studerus, A. Herrmann, and K. Ensslin, Rev. Sci. Instrum. **70**, 2765 (1999).

[28] F. Giessibl, Rev. Mod. Phys. **75**, 949 (2003).

[29] Y. Dubi, Y. Meir, and Y. Avishai, Phys. Rev. B **74**, 205314 (2006).

[30] S. A. Trugman, Phys. Rev. B **27**, 7539 (1983).

[31] B. Kramer, T. Ohtsuki, and S. Kettemann, Phys. Rep. **417**, 211 (2005).

[32] A. Baumgartner, T. Ihn, K. Ensslin, G. Papp, F. Peeters, K. Maranowski, and A. C. Gossard, Phys. Rev. B **74**, 165426 (2006).

[33] A. Pioda, S. Kičin, T. Ihn, M. Sigrist, A. Fuhrer, K. Ensslin, A. Weichselbaum, S. E. Ulloa, M. Reinwald, and W. Wegscheider, Phys. Rev. Lett. **93**, 216801 (2004).